TECHNICAL MEMORANDUMS

NATIONAL ADVISORY COMMITTEE FOR AERONAUTICS

No. 915

EXPERIMENTAL AND ANALYTICAL INVESTIGATION OF A MONOCOQUE WING MODEL LOADED IN BENDING

By E. Schapitz, H. Feller, and H. Köller

Luftfahrtforschung
Vol. 15, No. 12, December 10, 1938
Verlag von R. Oldenbourg, München und Berlin

Washington
October 1939

NATIONAL ADVISORY COMMITTEE FOR AERONAUTICS

TECHNICAL MEMORANDUM NO. 915

EXPERIMENTAL AND ANALYTICAL INVESTIGATION OF A MONOCOQUE WING MODEL LOADED IN BENDING*

By E. Schapitz, H. Feller, and H. Köller

Bending tests with transverse loads and with pure bending were undertaken on a double-web monocoque wing model in order to establish the relation between the state of stress and the results from the elementary bending theory. The longitudinal stresses in the stiffeners were measured with tensiometers and the shear stresses in the sheet were calculated from them. The measurements were made at both moderate loads with no buckles in the covering and also at loads with which the critical stress in the individual panels was exceeded. For the comparison, the wing skin was considered as stiffened sheet according to the shear panel scheme. In this way the statically indeterminate calculation was confirmed by the test results.

I. STATEMENT OF THE PROBLEM

The well-known type of aircraft construction in which not only the shearing forces but also the direct forces resulting from bending are resisted by the stiffened sheet covering is designated in a larger sense as the monocoque type. (See fig. 1, reference 1.) Such a construction offers advantages in respect to aerodynamic and weight considerations as compared to spar wings with torque tubes. The aerodynamic advantage consists in the fact that a wing shell stiffened by members in the direction of the span is generally stiffer in regard to buckling than a torque tube, which is stiffened only by a single auxiliary rib. Therefore, in the case of monocoque wings there is less danger that permanent buckles might occur in the covering and that the drag might increase (reference 2). The weight savings are effective only if at least one side of the wing can be built without openings (for tanks, engine nacelles, and the

*"Experimentelle und rechnerische Untersuchung eines auf Biegung belasteten Schalenflügelmodells." Luftfahrtforschung, vol. 15, no. 12, December 10, 1938, pp. 563-576.

like) and if the questions of fastening to the fuselage and the connection between the units, are solved satisfactorily. In this case it is especially important whether the wing construction in the neighborhood of the fuselage must be transformed into a spar construction. With shoulder covers and deep covers, for example, this can be given up and one can attach the individual stiffeners at the connections by means of screws. If, however, only a single strut is to be carried through the fuselage (for example, at the principal span), then the uniformly distributed longitudinal force in the wing shell must be transmitted to this point. The same problem arises as soon as the shell is interrupted by an opening.

For the investigation of the strength, one can resolve the questions arising in the monocoque wing into a series of individual problems. The influence of the single moment introduced at the point of attachment can be represented in such a way that one superposes the states of stress according to the ordinary bending theory and a group of forces in equilibrium (fig. 1). This equilibrium group decreases with increasing distance from the point of attachment. Another individual problem is the increase of stress in the stiffeners of a wing loaded by a transverse force at an opening if the deformation of the same is not restrained (fig. 1c). In these cases the longitudinal stiffeners in the interior are not active in the neighborhood of the application of the load on account of the absence of shear forces at the free edge; while, according to the simple theory of bending of beams, they should show a higher stress than the stiffeners at the spars because of their greater distance from the neutral axis. Figure 1c shows a third problem; Because of the shear flow* the built-in transverse cross section would warp out of its plane if it were not restrained by the supporting forces. Through this resistance to deformation, there occurs a group of normal forces in equilibrium whose effect vanishes at the free end. Similar disturbances arising from the restrained warping of the cross section are present in the case where the load is distributed along the length.

The tests on a monocoque wing model described in this paper are a basis for the experimental determination of the stress disturbances. The variation of the actual

*The term "shear flow" literally translated from "schubflüsse," appears to be used rather extensively in the German literature to denote shear stress times sheet thickness.

stresses from those obtained by the elementary theory of bending are taken as a measure of the stress disturbance. By introducing pure bending moment from couples, the stress disturbances from the application of concentrated loads were studied. By introducing concentrated loads at webs and distributed loads over the length of the shell, the effect of the restrained deformation of the cross section was studied. The measurements were therefore made at loads before as well as after buckling. The shear stresses were determined from the test results in a manner similar to that carried out for a stiffened circular cylinder in an earlier investigation (reference 3).

The individual problems studied can be treated theoretically also with the methods for the calculation of statically indeterminate systems by making simplifying assumptions. For the stiffened sheet, of which the monocoque wing is made, the process of calculation is carried out in a work by Ebner and Köller (reference 4). In it the sheet field is considered to resist shear only and the normal forces are considered concentrated in the longitudinal and transverse stiffeners. The strength of the skin is taken into consideration by the addition of an effective width to the cross section of the stiffener. In the case of tests of a circular cylinder loaded at a single point (see reference 3), it has been established that the calculations, according to this "shear-field theory," give a very good agreement with the measured values for stiffened complete shells (reference 5). The stress measurements presented herein can only serve to prove the applicability of the shear-field theory to the calculation of stiffened sheet. In section IV the procedure of calculation is shown and a comparison between the calculated and measured stresses is made.

II. TEST SPECIMEN, TEST PROCEDURE, AND LOADING CONDITIONS

The test specimen, which is described briefly in an article by H. Ebner (see reference 1, pp. 185-186*) represents the interior section of a double-web monocoque wing. Its statical tension side (under side) is, in the case of this first model, concentrated into two heavy chords on the webs (fig. 2). The model represents therefore a trough, whose open side is turned upward because of the greater

*The model and the arrangements for loading and supporting were built by Dr. Ing. Lücker.

convenience in the work. While testing, the model is therefore reversed from the position in the actual wing (compressive side down). The model, as an open trough, facilitated the stress measurements appreciably; it is used in similar form also in the case of American investigations (reference 6). The tension chords, consisting of formed duralumin sheet, each of 15 cm^2 (2.325 sq. in.) cross section, are attached with screws to the angles of the spars, in order that a tension skin could be used in its place later.

The compression side consists of a sheet covering 1.2 mm (0.0186 in.) in thickness, with a radius of curvature of 4,000 mm (157.5 in.). It is stiffened with closed hat-shaped stiffeners spaced 140 mm (5.51 in.). The clear width of sheet between the rivet rows is 90 mm (3.54 in.). The center stiffener is composed of two C-shaped sections. At the edges, the covering is joined by two heavy angles to the spar webs. Figure 3 shows the dimensions and cross-sectional areas of these longitudinal stiffeners. The average sheet thickness (total cross section without spar angles, expressed in units of arc length) of the compression side defined by the inner rows of rivets at the spar angles 1 and 9, is 2.75 mm (0.082 in.), thus the cross section is distributed 43.5 percent to the skin and 56.5 percent to the stiffeners.

The spar web is 3 mm (0.118 in.) thick and so proportioned that the spar can remain flat until failure in the case of an ultimate load test with transverse bending loads. In the region of the fixed end, the web is provided with longitudinal stiffeners in order to increase the resistance to buckling (reference 7).

The position of the centroid S of the whole cross section is indicated in figure 2. The moment of inertia of the cross section referred to the transverse axis through S is $J = 24{,}300$ cm^4 (583.8 $in.^4$). The distance z of the centroid of the stiffener S_g from the transverse axis through S (see fig. 13) is given in table I.

As transverse stiffeners, there are cross frames spaced a distance of 500 mm (14.69 in.). The cross-frame chords consist of hat-shaped sections of 1.5 cm^2 (0.233 sq. in.) cross section; the posts and diagonals are C-shaped sections of 2.3 cm^2 (0.357 sq. in.) and 0.8 cm^2 (0.124 sq. in.), respectively. The transverse frames are attached by special angles at the spar stiffeners. At the

spars they are riveted so that their posts together with the web stiffener lying on the outside, stiffen the web sheet. The designation of the spaces and the transverse joints is shown in figure 2.

TABLE I. Distances, z, of the Centroids of the Stiffeners, S_g, from the Transverse Axis through the Centroid of the Section, S

Stiffener i	1 and 9	2 and 8	3 and 7	4 and 6	5	10 and 11
a) z_i =	14.7 5.79	15.9 6.26	17.1 6.73	17.8 7.01	17.7 6.97	16.9 cm 6.65 in.
b) z_i =	14.8 5.83	16.3 6.42	17.5 6.89	18.2 7.17	18.2 7.17	16.9 cm 6.65 in.

a) S_g refers to the stiffener with the strip of sheet between the rivets.

b) S_g refers to the stiffener with a strip of sheet equal to half the spacing on each side.

For supporting the model, use is made of a frame (fig. 4) which is self-contained and can support bending loads without the aid of a foundation. The spar chords and the skin in the compression zone are attached through an angle at the edge to a heavy steel plate. Wedges are used to transfer the compressive force from the longitudinal stiffeners to the steel plate. By this means, a uniform bearing of the stiffeners on the plate can be obtained. (See fig. 5 for the attachment described.) The compression sheet is reinforced directly at the fastening by a fishplate in order to exclude as much as possible a failure directly at the point of application of the load. The two tension chords are carried as fishplates through the heavy steel plate and fastened by means of turned bolts to a box beam arranged between the supports of the loading frame.

For the loading of the model, it is provided that at each web both a concentrated load at the free end and also a smaller transverse load can be applied at each cross frame. Further, however, pure bending moments in various planes can be introduced at the free end and, indeed, at both webs and at the center of the model. For applying the moments, use is made of a loading device (which has

been described (reference 8) previously), which consists of a loading triangle and an attached rectangular link (fig. 4). The tensile forces are transmitted to the concentrated tension chords by means of a transverse member (see figs. 6c and 6d) while the compressive forces act through a loading beam to the group of stiffeners. In the case of applying the moments over the webs, stiffeners 1 and 9 (fig. 6) are loaded and when moment is applied at the center of the section, stiffeners 4, 5, and 6 are loaded. Figure 5 shows the assembly for applying load at this point. For applying the distributed load at the cross frames, the web is carried below the edge angle and is equipped with rings; the load is provided by dead weights. The concentrated loads at the free ends of the webs are applied by a screw jack which acts through a dynamometer onto the web (fig. 4).

The arrangement of the measuring stations on the transverse sections of the wing model and the stations on the stiffeners is shown in figure 2. Huggenberger tensiometers with a multiplication ratio of 1:1,100 were used as measuring instruments. The original gage length of 20 mm (0.787 in.) was increased in consideration of the small strains to be measured to 100 mm (3.94 in.) by means of attachments. Since temperature changes, especially by the sun's rays, have a great influence on the measurements, the temperature was controlled continuously by a thermostat. The greatest permissible temperature change during a series of measurements amounted to $\pm 0.5^{\circ}$ C.

The tests related to the loading conditions shown in figure 6. The first case concerns the application of two equal transverse loads at the free ends of the webs with free longitudinal distortion of the loaded cross sections. In the second case, transverse loads whose total magnitude equaled the load applied at the free ends in the first case, were applied at the intermediate transverse frames. With this loading, the influence of the restraint to distortion at the fixed end, according to figure 1c, should be studied. Since beyond the first load point there is an unstressed field, there is also a restraint to distortion of the cross section in the first panel (fig. 6b). The third case concerns the application of a couple at each web with free distortion of the cross section at the loaded end and uniform support at the built-in end. (See fig. 6c.) In the last case (fig. 6d) a single moment is applied at the center of the wing with the same conditions of distortion as in the third case.

III. TEST RESULTS AND THEIR EVALUATION

1. The Stress Peaks in the Four Loading Cases before the Buckling of the Covering

The results of the strain measurements at the individual measuring stations were interpreted into stresses with an elastic modulus, E, equal to 740,000 kg per cm^2 (10,525,000 lb. per sq. in.), which is an average value from various test specimens. Under the assumption of linear distribution of stress across the section of the stiffener, the stress at the centroid (σ_L) of each longitudinal stiffener was determined from the values of stress at the individual gage lines. These centroidal stresses are shown in figures 18, 21, and 23 for comparison with the values calculated by the shear-field theory. In order to give a clear picture of the test results, smooth curves were drawn through the measured values which are shown in perspective in the following figures.

a) Application of a single load at the free ends of the webs.- In figure 7 the centroidal stresses, σ_L, of the longitudinal stiffeners are plotted on the wing span (coordinate x) and the wing width (coordinate y). The distribution given by the elementary bending theory is shown by the light lines; stresses increasing linearly with x and decreasing with y from the center out to the webs because of the curvature of the skin covering. The figure clearly shows two variations in the courses of the curves: At the free end (loaded end), the increment of stress in the x-direction in the interior stiffeners disappears while in the edge stiffeners at the web the increment is greater than that according to the elementary bending theory. At the fixed end, the stress peaks are over the webs and a decrease in stress toward the middle is to be noticed, so that the σ_L curves in the transverse direction are curved opposite to those from the elementary theory.

The variation at the free end arises from the fact that there, because of a lack of edge stiffening, the shear stresses in the skin must vanish. Since an increase in stress in a stiffener can result only by the occurrence of shear forces in the web or in the covering, then no increase in stress at the free ends of the interior longitudinal stiffeners is possible. The middle of the wing, therefore, is only a little effective in the first panel. The variation at the fixed end is explainable, on the other hand,

from a restraint to distortion of the cross section: because of the transverse forces, the cross section would assume the distorted form indicated in the smaller sketch of figure 1c; since plane sections must remain plane at the built-in end, then there arises a group of forces which are in equilibrium. They consist of additional compressive forces at the lower spar chords and tensile stresses in the middle. Their effect decreases in the longitudinal direction so that at the middle of the model (about 1,500 mm (59.06 in.) from the point of application of the load) the stress distribution corresponds to the elementary bending theory.

b) Loading of the webs by load distributed over the length of the wing.- Figure 8 shows the stress peaks corresponding to the case in which the transverse load is applied, not as a concentrated load at the free end but as a uniform load distributed over the length of the wing. The total transverse load is the same as in case a). The stress distribution according to the elementary theory is parabolic and the diagram is made up of straight lines between the cross frames; over the width of the wing (y-direction) there is an increase from the edges toward the center as was expected previously. Also in this loading case there are variations at both ends; at the unloaded free end, tensile stresses arise in the spar chords on the compression side and in the center the compressive stresses are higher than according to the elementary theory. At the built-in end, stress peaks at the spar chords and a decrease in the stress at the center appear as in case a).

The variance at the built-in end results from the restraint to distortion of the cross section as in case a), only the effect is relatively greater because the same shear force and same secondary stress arising therefrom stand in contrast to a smaller bending moment. The variance at the unloaded free end is opposite in direction to the variance at the same place in case a) and is brought about by the fact that beyond the last point of application of the load, there is an unloaded wing member which restrains the distortion of the foremost cross section. The accompanying internal state of stress is the same except for magnitude and sign as at the built-in end; compressive stresses are produced in the middle of the wing and tensile stresses at the webs.

c) Loading by concentrated couples of pure bending moment.- Figure 9 shows the stress peaks for the case of

pure bending if the moment is applied at the loaded end as a couple concentrated at the webs. The elementary theory would give a constant stress over the length of the member. A variance enters in this case only at the points of application of the forces since no shear forces are transferred and therefore the cross sections are free of shearing stresses at a sufficient distance from the point of application of the load. In consequence of this, the cross sections, free to distort, remain plane.

At the loaded end, the compressive stresses are concentrated in the spars at the points of application of the forces. The longitudinal stiffeners in the middle are nearly free of stress and near the edge also no increase of stress is shown since here the shear stresses vanish. The equalization to the elementary distribution of stress occurs within four panels (between the cross frames).*

An accordingly similar process occurs if a couple is applied at the middle of the wing (fig. 10). The compressive forces were applied to the three middle ribs 4, 5, and 6 by the loading arrangement represented in figure 5. The initial stress in ribs 4 and 6 is somewhat smaller than that in number 5 because of the flexibility of the loading bar. The equalization to the elementary distribution in the case of applying the load at such an unusually weak spot occurs in about the same distance along the wing as in the previous case with the application of the moments at the webs.

2. The Effect of Buckling of the Skin on the Curves of the Longitudinal Stresses

Since the pattern of the stress distribution must be calculated for the buckled as well as the unbuckled skin, the previously described stress measurements were extended into the range of buckling. The upper limit of the load range was therefore determined from a consideration of the strength of the stiffeners and the tendency to buckle; permanent buckles in the skin were to be avoided as much as possible because of the succeeding measurements. For the several loading cases, the loads at which the buckles were first noticed were exceeded by the following amounts:

Load case	Degree of excess
Transverse force at the free ends of the webs	2.25
Pure bending, moment at the ends of the webs	2.00
Pure bending, moment in the middle	1.90

*This loading case corresponds to that studied by Lovett and Rodee. (See reference 6.)

In the case of the distributed transverse load the buckling region was not investigated.

The effect of the buckles on the stress distribution consisted in a diminution both of the compressive stiffness (the effective width) and the shear stiffness of the skin. This effect will be shown by means of the measurements for the several loading cases. Thus the stresses were reduced to a basis of a unit load in order to be able to make a direct comparison. Further, for clear plotting, the stresses were multiplied by the cross section of the longitudinal stiffeners (stiffener plus the adjacent sheet between the rows of rivets); thereby the force P_x was obtained without consideration of the adjoining sheet panel.

When the wing supports a concentrated load at the free end, the skin in the neighborhood of the built-in end buckles because the moment increases over the length while at the loaded end the sheet remains unbuckled. Figure 11 shows the longitudinal stresses corresponding to the unit load of 1,000 kg (2,204.62 lb.) at the free end, plotted as a group of curves on the length of the wing. One notices that the variation at the built-in end is somewhat more marked after buckling than before. This results, on the one hand, from the decreased shear stiffness of the skin which leads to greater distortion and to greater secondary stress; on the other hand, the smaller effective width in the buckled state counteracts this effect and leads in the case of equal forces to greater stresses in the stiffeners. That all effects act together can be seen from the fact that the longitudinal stresses in the stiffeners in the central portion of the wing after buckling are in part greater and in part smaller than before buckling. An approximate mathematical representation of this interdependence will be shown in section IV.

In the case of the loading with pure bending by couples in the planes of the webs, only the strips of covering directly against the chord angles of the spars buckled in the limited load range. The effect on the vanishing point was unimportant and not to be recognized in the scatter of the data points. (See, for example, fig. 11.) With the application of the couples on the three interior stiffeners (4, 5, 6, fig. 12), a definite increase in the stresses is apparent in the latter in comparison with the state before buckling (reduced to a unit load of 1,000 kg on a lever arm of 89 cm). This effect is clearly traceable to the decrease in the effective width in the cover-

ing sheet; the load curves for the remaining stiffeners remain unchanged since the buckling was limited to the highly stressed sheet in the region from stiffeners 4 to 6. Also in figure 12, the distribution of the data points follow the faired curves.

3. Shear Flow

a) Computations based on the measured longitudinal stresses.- The measured longitudinal stresses can be used to determine the distribution of the shear stresses in the load range before buckling. One obtains, thus, an insight into the shear loading of the skin of the wing shell in the neighborhood of the points of application of loads and fixation. Furthermore, this evaluation is important in making the comparison with the calculations according to the shear-field scheme.

In this way, the stiffness under axial loads of the stiffeners and of the sheet covering are assumed concentrated in the longitudinal and transverse stiffeners; therefore, the shear stress within a panel of the skin is constant and can change abruptly only at the stiffeners and the cross frames. If the transverse frames are not joined directly to the covering, then one can consider either the stiffness under axial load (through the lateral bending stiffness of the longitudinal stiffeners) divided uniformly over the skin and thus obtain a system with closely spaced cross frames, or one concentrates the shear stiffness of the adjacent half panel with the stiffness under axial load of the cross frames into a single imaginary frame joined to the skin. In the first case, the shear flow $t = s$ changes steadily in each longitudinal strip and only at the stiffeners do abrupt changes occur; in the second case, the shear flow likewise changes abruptly at the separate cross frames and is constant within the panel. The comparison with the shear flow obtained in the tests shows then to what extent these calculated average values of shear flow approximate the actual distribution.

Since the longitudinal stresses in the skin were measured only at the changes in the section, it is necessary to make an assumption of the distribution of the longitudinal stresses over the cross section of the sheet in order to make a complete computation of the shear flow. It is approximate to try a variation within a single panel that is linear between the stresses measured at the edges of the panel. A comparison of the external bending moment

with the resisting moment calculated from the measured stresses shows that this assumption of the effectiveness of the full width of sheet between two longitudinal stiffeners in the load range before buckling leads to small differences from the state of equilibrium. Table II shows the distribution of the resisting moment for section VIβ (near the application of the forces) which lies in the region of greatest variation of stress. The moments of the stresses in the skin were calculated according to the above assumption concerning the longitudinal stresses. It shows a satisfactory agreement between the external and resisting moments.

TABLE II. Comparison of the External Bending Moment with the Resisting Moment from the Longitudinal Stresses Measured at Section VIβ

Loading case	Moment of the longitudinal forces, P_x mkg	Moment of each stiffener mkg	Moment of the web mkg	Moment of the skin mkg	Sum of internal moments mkg	External moment mkg
Couples at the webs	2,225	21	287	176	2,709	2,714
Couple at the middle	2,084	25	126	411	2,646	2,714

Moment in mkg times 86.81 equals moment in inch-pounds.

For the determination of the shear flow from the centroidal stresses, σ_L, the longitudinal forces, P_x, in the stiffeners (stiffener plus the adjacent strip of sheet between the rivet rows) were determined and were joined by a faired curve over the length of the wing. The relation

$$\frac{d\,P_x}{dx} = P_x' = t_r - t_l \qquad (1)$$

obtained from the condition of equilibrium of an element of the member exists between the changes in the longitudinal force, P_x, in a stiffener across the width of the

wing (coordinate x) and the shear flow, t_l and t_r (concerning the designations, see fig. 13) in the panels adjacent to the stiffener. By graphical differentiation of the faired P_x curve, one obtains by means of equation (1) the difference in the shear flow in the adjacent panels at each cross section and at each longitudinal stiffener. The plane of symmetry of the model through stiffener 5 is also a plane of symmetry for the longitudinal stresses in all the loading cases. The shear stresses must therefore always be antisymmetric with respect to it. One obtains therefore by means of equation (1) from one-half the P_x curve for the middle stiffener, 5, the amount of the shear flow which occurs on each side of the longitudinal stiffener. If the four panels in one-half of the shell are designated 1, 2, 3, amd 4, the edges with the indices l and r in the direction of the stiffener numbering (fig. 13) and the shear flow at the lower edges of the webs with t_{s_u}, then it follows from (1) that

$$\left.\begin{aligned} P'_{x5} &= 2t_{4r} \\ P'_{x4} &= t_{3r} - t_{4l} \\ P'_{x3} &= t_{2r} - t_{3l} \\ P'_{x2} &= t_{1r} - t_{2l} \\ P'_{x1} &= t_{s_u} - t_{1l} \end{aligned}\right\} \quad \ldots\ldots\ldots\ldots (2)$$

The distribution of shear flow in the sheet panels and with it the relation between t_{4r} and t_{4l}, t_{3r} and t_{3l}, etc., are found by the integration of the equation of equilibrium of the elements of the skin

$$\frac{\partial \sigma_x}{\partial x} + \frac{\partial \tau}{\partial y} = 0$$

whereat a linear variation over the panel width, b, between the edge values of σ_{xl} and σ_{xr} is assumed for σ_x, therefore

$$\sigma_x = \sigma_{xl} + (\sigma_{xr} - \sigma_{xl}) \frac{y}{b} \qquad (3)$$

(y in each panel is measured from the left.)

From this it follows by differentiation with respect to x

$$\frac{\partial \tau}{\partial y} = -\frac{\partial \sigma_x}{\partial x} = -\frac{d\sigma_{xl}}{dx} - \left(\frac{d\sigma_{xr}}{dx} - \frac{d\sigma_{xl}}{dx}\right)\frac{y}{b}$$

and by integration with respect to y

$$\tau(x,y) = \tau(x,0) - \frac{d\sigma_{xl}}{dx}\,y - \left(\frac{d\sigma_{xr}}{dx} - \frac{d\sigma_{xl}}{dx}\right)\frac{y^2}{2b} \qquad (4)$$

The shear stress is therefore parabolic over the cross section in each panel. The difference in the shear flow between the edges l and r of a panel is

$$t_r - t_l = -\frac{bs}{2}\left(\frac{d\sigma_{xr}}{dx} + \frac{d\sigma_{xl}}{dx}\right) \qquad (5)$$

The terms $\frac{d\sigma_{xr}}{dx}$ and $\frac{d\sigma_{xl}}{dx}$ for the individual panels are obtained from the measured stresses in the skin at the stiffeners which are joined by a faired curve and then the derivatives are determined graphically at the sections studied. Now if a summation is made, from the middle out to the edge at a certain cross section, of the differences in shear flow calculated according to (2) and (5), a curve for the variation in the shear flow is obtained for the cross section under consideration. It consists of parabolic segments over the free width of the sheet according to equation (4); at each stiffener there is a discontinuity according to (2). If the skin stresses on both sides of the stiffener agree, then the adjacent parabolic segments have the same slope. The discontinuity at the stiffener can then be divided into two separate discontinuities of equal magnitude at the rows of rivets, whereat the shear flow in the strip of skin under the stiffener varies as a straight line in the direction of the ends of the tangents of the adjacent parabolic segments. (See figs. 14 to 17.)

If P_{xZ} is the force in the tension chord (fig. 2), then the shear flow, t_{S_o}, at the upper edge of the web is computed from

$$t_{S_o} = -\frac{dP_{xZ}}{dx} \qquad (2a)$$

For the web (height, h, between the centroids of the

chords), equation (5) can be rewritten in the following manner:

$$t_{S_o} - t_{S_u} = \frac{hs_S}{2}\left[\frac{1}{F_1}\frac{dP_{x_1}}{dx} + \frac{1}{F_Z}\frac{dP_{xZ}}{dx}\right] \qquad (5a)$$

in which s_S is thickness of web

F_1, cross-sectional area of the lower chord angle

F_Z, cross-sectional area of the tension chord

The relation (5a) can serve as a check since the evaluation of the shear flow, t_{S_u}, obtained by means of (2) and (4) through the summation on the compressive side must lead to the same result as obtained according to (2a) and (5a) for the tension side.

b) The shear flow in the loading cases studied.- The shear flow in the loading cases studied was determined according to this process of calculation for the sections where stresses were measured. The results are shown in figures 14 to 16; the absolute amounts of the shear flow (for the measuring stations shown) are plotted over the half cross section. The check described for t_{S_u} is carried out in all cases; the maximum variation is 8 percent, which is traceable to the arbitrariness in the choice of the adjusted curve through the scattered data points and to the errors in the graphical differentiation.

Of the four loading cases studied: bending with transverse forces (with concentrated loads at the free end and with loads distributed over the length) and pure bending (with forces applied at the webs and forces applied in the middle) - the last two cases differed from the first two in such a way that the elementary stress distribution gave no shear flow; therefore, shear stresses are traceable only to the distortions resulting from the application of concentrated loads. The two cases of bending with transverse forces are different, in that in the case of the concentrated load at the free end the total shear force to the absorbed over the width x remains constant while for the distributed load it increases toward the built-in end. The localized stresses at the points of fixation and at the application of the loads produce a distortion of the distribution of the shear flow.

In the case of bending with concentrated loads at the free end (fig. 14), the total shear flow in the web is concentrated, at first, behind the point of application of the load because the longitudinal stiffeners (except 1 and 9) are not active. After that, the shear flow in field VI rises very rapidly because this field must transfer the total shear for the stress increments in the interior stiffeners. With the approach of the longitudinal stresses to the linear variation, the shear flow decreases over the whole width. The distortion at the fixed end causes a strong decrease in the shears over the whole width of the wing (see left side of fig. 14) because the buckling stresses unload the inner panels and stiffeners so that the increases in the forces and the accompanying differences in shear flow from field to field are smaller.

In the case of bending with distributed load (fig. 15) the increasing transverse force corresponding to the shear increases from the free end to the fixed end until the distortion resulting from the buckling forces at the fixed end again cause a decrease which is more noticeable in the interior panels than in those near the webs. The increase in the normal stresses in these panels is (see fig. 8) noticeably greater than in the interior panels. The reverse changes in the shear curves for cross sections $I\alpha$ and $I\beta$ at the built-in end are caused by the fact that the individual bending of the longitudinal stiffeners at these points unloaded the backs of the stiffeners and the sheet stresses increased accordingly.

In the case of pure bending with the forces applied at the webs (fig. 16), the shear reduces to zero with approach to the built-in end; it fades out steadily at all sections from the web toward the center. In the case of the application of the load at the center (fig. 17), the shear attains its greatest value in the foremost cross section in the panels which are directly outside the loaded stiffeners, 4 and 6. At a greater distance from the points of application of the load, these maxima flatten out and the shear flow vanishes at the built-in end.

IV. CALCULATION OF THE STRESS DISTRIBUTION ACCORDING TO THE SHEAR FIELD CONCEPT

1. Basis of the Statically Indeterminate Calculation

The stress distribution for the loading cases studied experimentally will be determined mathematically with the assumption that the skin resists only shear as in the procedure developed in an earlier work by Ebner and Koller (reference 4). This work is referred to later by the abbreviation E-K.

The longitudinal forces in the stiffeners and the adjacent strips of sheet are considered concentrated at the centroids of the stiffeners;* the stiffness of the skin under axial loads is considered as an increase in the stiffness of the stiffener. Let it be assumed that the covering is not buckled at first. Then one-half the sheet panel on each side of the intermediate stiffeners is to be added. The web sheets are also regarded as being purely shear resistant with a height $h = 30$ cm (11.81 in.), and a thickness of $s_S = 0.3$ cm (0.118 in.). In order to obtain the same stresses in the stiffeners at the webs of the idealized system as in the actual model, it is necessary to add to that stiffener area an effective web area of $\frac{1}{6} h s_S = 1.5$ cm^2 (0.233 sq. in.). Under these assumptions, one obtains, with the dimensions from figures 2 and 3, the following effective stiffener areas:

$F_1 = F_9 = 7.4$ cm^2 (1.147 sq. in.)

$F_2 = F_3 = F_4 = F_6 = F_7 = F_8 = 3.8$ cm^2 (0.589 sq. in.)

$F_5 = 5.0$ cm^2 (0.775 sq. in.)

$F_{10} = F_{11} = 20.9$ cm^2 (3.240 sq. in.)

The simplified system of stiffeners with these cross-sectional areas, which are joined only by a shear resistant sheet, occupies the same centroids as the actual model and their moments of inertia differ by only about 2 percent from the actual values.

Let it be further assumed that the fixation of the model occurs at cross frame a (see fig. 2) since the

*These longitudinal forces differ therefore from the earlier values P_x, which designated only the forces in the stiffeners directly in contact with the skin.

23.5 cm (9.25 in.) extension at the point of fixation is reinforced by the angle along the edge and a strip of sheet on the compression side. The end frame a is assumed as rigid. The transverse stiffness of the compression sheet is composed of the stiffness of the skin to axial load in the transverse direction and that of the chords of the transverse frames, which are not joined directly to the skin. It is assumed that the stiffness under axial load of the cross frame serves only to equalize the forces resulting from the curvature of the compression side and therefore the full transverse stiffness of the covering is effective in the shell. For the case of bending with transverse forces, the normal forces in the transverse direction and the transverse stiffness of the skin are considered concentrated in the transverse stiffeners joined to the skin at the distance $a = 50$ cm (18.68 in.), with an effective cross-sectional area $F_S = 50 \times 0.12 = 6.0$ cm^2 (0.930 sq. in.). In the case of pure bending, on the other hand, $F_S E = E\ 0.12$ cm ($E\ 0.0472$ in.) is computed with the distributed transverse stiffness because for this problem complete solutions of the equations of elasticity apply in the limiting case of heavy frames.

The compression side of the wing model including the spar chords represents, under these assumptions, a stiffened shell with nine stiffeners as they are treated in reference 4. The average spacing of stiffeners, b, is 13.8 cm (5.43 in.); the skin thickness, s, 0.12 cm (0.0472 in.); and the value of G/E is 0.385. Equation (18) of E-K then gives the following values:

$$\omega_L = \frac{1}{3}; \quad \omega_B = \frac{b}{s\sqrt{G/E}} = 298.7; \quad \omega_S = \frac{b^3}{aF_S} = 8{,}760 \qquad (6)$$

The orthogonal characteristic force groups $\underline{X}_{\mu_k}$ of a regular shell with equal stiffeners are chosen as static redundants; the partial forces are taken from table I of E-K for $m = 9$. They are given in table III, also the corresponding $\kappa\omega$ values from which the shearing coefficients of the elastic equations can be evaluated. The values of κ_B and κ_S are taken from table I of E-K and multiplied by the corresponding values of ω from (6); the values of κ_L are determined exactly according to equation (19) of E-K.

$$\kappa_L = \left(\frac{a}{2}\right)^2 \sum_{i=1}^{9} \frac{P_i^{(\mu)}\ P_i^{(\mu)}}{F_i}$$

because the attached stiffeners are not all alike. In the setting up of the elastic equations, therefore, besides the coupling terms resulting from the strains in the cross frames, there are also such terms resulting from the longitudinal stiffeners which are also neglected; that is, the values X of the redundant characteristic force groups are determined from independent 5-term equations. (See E-K, example.) On account of the curvature of the compression side, bearing stresses arise at the webs as a result of the characteristic force groups, as is brought out in section IV of E-K. Since the curvature is small, its effect in the loading cases with transverse bending forces is neglected. With the introduction of couples, on the other hand, they must be considered because herewith the redundants assume rather large values.

TABLE III

Partial Forces and Shear Coefficients of the Statically Redundant Characteristic Force Groups

Redundant	Partial forces $P_i^{(\mu)}$					$\kappa_L \omega_L$	$\kappa_B \omega_B$	$\kappa_S \omega_S$
	i=1 and 9	2 and 8	3 and 7	4 and 6	5			
$\underline{X}_{1k}$	-0.940	-0.500	0.174	0.766	1	186.5	2873	1936
$\underline{X}_{2k}$	.766	-.500	-.940	.174	1	202.3	813	109.6
$\underline{X}_{3k}$	-.500	1.000	-.500	-.500	1	220.1	448	17.52
$\underline{X}_{4k}$	.174	-.500	.766	-.940	1	232.0	346	4.34

With the carrying out of the statically indeterminate computations, a few designations are changed from those used in the previous sections and also in comparison with the work of E-K. The transverse frames and the corresponding redundants are designated with digits 0, 1, ..., 6 from the free end instead of with letters g, f, ..., a; the index k indicates, generally, one of these frames. (See fig. 2, numbers in parentheses.) The stiffener numbering begins at the spars with 1, 2, ...; the sheet panel between the stiffeners carries the number of the stiffener on the left (fig. 13).

2. Stress Distribution in the Case of Transverse Bending Forces

Let the transverse stiffness of the compression side be concentrated in the individual frames 0, 1, ..., 6, which are joined to the skin. Frames 0 to 5 have the same cross section $F_S = 6.0$ cm^2 (0.930 sq. in.). (Frame 6 is rigid.) Since the extension at the free end, with a length of 23.5 cm (9.25 in.), is not closed by a frame, then on the basis of the shear-field notion there can be no longitudinal stress in the field between the stiffeners and with it no redundant at the frame 0. At frames 1 to 6, characteristic force groups $\underline{X}_{\mu k}$ produce the necessary internal state of stress in the stiffened shell, whose multiples $X_{\mu k}$ are calculated from the independent equations of elasticity. The coefficients of the equations of elasticity are obtained from the values of $\kappa\omega$ in table III, according to equation (17) of E-K, whereby it is considered that the rigid frame 6 produces no contribution, and the redundant $\underline{X}_{\mu 6}$ effective there applies to the shear field only. It is then

$$aE\delta_{kk} = 8\kappa_L\omega_L + 2\kappa_B\omega_B + \tfrac{3}{2}\kappa_S\omega_S \quad \text{for } k = 1, 2, 3, 4$$

$$aE\delta_{55} = 8\kappa_L\omega_L + 2\kappa_B\omega_B + \tfrac{5}{4}\kappa_S\omega_S$$

$$aE\delta_{66} = 4\kappa_L\omega_L + \kappa_B\omega_B + \kappa_S\omega_S$$

$$aE\delta_{k,k-1} = 2\kappa_L\omega_L - \kappa_B\omega_B - \kappa_S\omega_S \quad \text{for } k = 2, 3, 4, 5$$

$$aE\delta_{65} = 2\kappa_L\omega_L - \kappa_B\omega_B - \tfrac{1}{2}\kappa_S\omega_S$$

$$aE\delta_{k,k-2} = \tfrac{1}{4}\kappa_S\omega_S \quad \text{for } k = 3, 4, 5, 6$$

The δ values multiplied by $c = aE\,10^{-2}$ are assembled in tables IV to VII.

As a principal substitute system for the external loading, the "ideal beam" whose state of stress is obtained from the elementary theory of bending, is taken as a basis. The internal state of stress of the characteristic force groups then gives the deviations from this simple distribution which arise from the restrained distortion of the cross section at the built-in end and at the points of application of the loads.

Loading case a, concentrated load at the free end: The transverse load, $\bar{Q}$, half to each web, acts at the free end. The bending moment at the k^{th} frame amounts to

$$M_k = (ka + 23.5 \text{ cm})\ \bar{Q}$$

$$M_k = (ka + 9.25 \text{ in.})\ \bar{Q}$$

With the distances to the centers of gravity of the stiffeners, z_i, in table Ib, one obtains the distribution of force according to the elementary theory

$$P_{ik}^{(o)} = - (k\,a + 23.5 \text{ cm})\ \frac{F_i z_i}{J}\ \bar{Q}$$

$$P_{ik}^{(o)} = - (k\,a + 9.25 \text{ in.})\ \frac{F_i z_i}{J}\ \bar{Q}$$

and the corresponding shear flow, constant over the length,

$$t_{4k}^{(o)} = - t_{5k}^{(o)} = - \frac{1}{2}\ \frac{F_5 z_5}{J}\ \bar{Q}$$

$$t_{3k}^{(o)} = - t_{6k}^{(o)} = - \frac{\frac{1}{2} F_5 z_5 + F_4 z_4}{J}\ \bar{Q}$$

etc.

For $\bar{Q}$ = 1 kg (2.205 lb.), the values of shear flow multiplied by J are given in table VIII. Since these shear flows are constant in the longitudinal direction, they load only the two end frames, 0 and 6. Table VIII gives the values of the forces $Q_{oi}^{(o)}$ multiplied by J/b for frame 0 at the i^{th} stiffener resulting from $\bar{Q}$ = 1 kg (2.205 lb.), which are obtained by summing up the values $J\,t_{ik}^{(o)}$ from the edges. The corresponding values resulting from the redundants are also summarized in table VIII. (See section III of E-K.)

In this principal substitute system, the longitudinal forces $P_{ik}^{(o)}$ make no contribution to the loading terms in the equations of elasticity because they are determined under the assumption that plane sections remain plane, so that through them there arises no distortion of the cross sections and therewith no additional work by the forces of

the static redundants.* From the shear flow which is constant over the length there enters a loading factor different from zero only for the redundant $\underline{X}_{\mu 6}$ at the built-in frame:

$$\delta_{60}^{(\mu)} = \frac{2}{aE} \sum_{i=1}^{4} \frac{ab}{Js\ G/E} \left(a\ t_{ik}^{(\mu)}\right) \left(J\ t_{ik}^{(o)}\right)$$

Since frame 6 is rigid, then only the end frame (0) yields loading factors and, indeed, only for the redundant $\underline{X}_{\mu 1}$

$$\delta_{10}^{(\mu)} = -\frac{2}{aE} \frac{b^3}{6FsJ} \left[\frac{J}{b} Q_{02}^{(o)} \left(4\underline{R}_{k2}^{(\mu)} + \underline{R}_{k3}^{(\mu)} \right) \right.$$

$$+ \frac{J}{b} Q_{03}^{(o)} \left(\underline{R}_{k2}^{(\mu)} + 2\underline{R}_{k3}^{(\mu)} + \underline{R}_{k4}^{(\mu)} \right) +$$

$$\left. \frac{J}{b} Q_{04}^{(o)} \left(\underline{R}_{k3}^{(\mu)} + 2\underline{R}_{k4}^{(\mu)} + \underline{R}_{k5}^{(\mu)} \right) + \frac{J}{b} Q_{05}^{(o)} \left(\underline{R}_{k4}^{(\mu)} + 2\underline{R}_{k5}^{(\mu)} \right) \right]$$

If one inserts the numerical values of the dimensions as given previously and uses table VIII, then the loading terms (multiplied by $C = a\ E\ 10^{-2}$) contained in tables IV to VII inclusive, are obtained for $Q = 1$ kg (2.205 lb.).

The solution of the 5-term equations is carried out according to a usable system and the results are given in table IX. One recognizes from the equations of elasticity that the transverse stiffness is of importance only for the characteristic force group $\underline{X}_{1k}$, and further, that these redundants are appreciably greater than the other groups. In this way, the disregarded coupling with the force groups of higher order is small and is nonessential for the final force distribution.

By superposition of the values for the redundants from table IX, one obtains the force

*Because of the curvature of the sheet, the summations $\sum_{i=1}^{9} \frac{P_i^{(o)}\ P_i^{(\mu)}}{E\ F_i}$ were not equal to zero. If one considers, however, the effect of the supporting forces, the characteristic force groups in the curved sheet occur in the attached spars (see section IV of E-K), so the contribution of this work vanishes.

$$P_{ik} = P_{ik}^{(o)} + \sum_{\mu=1}^{4} P_{ik}^{(\mu)} X_{\mu k}$$

and, by division by the effective cross section of the stiffener, one obtains the centroidal stresses in the stiffeners at the cross frames. In figure 18, these stresses are plotted along the length of each stiffener for the load Q = 1,700 kg (3,749 lb.). According to the idealized model with the cross frames attached to the skin, they must be joined by straight lines. Since the actual frames are not located in the skin, then the shear in each longitudinal strip changes regularly and the values of the stresses at the frames are therefore to be adjusted by a smooth curve. For comparison, the centroidal stresses determined from the measurements are plotted in figure 18. It can be seen that the distortion of the elementary stress distribution is well represented by the statically indeterminate calculations.

The distribution of shear flow follows by superposition from table VIII, and the values for the redundants:

$$t_{ik} = t_{ik}^{(o)} + \sum_{\mu=1}^{4} t_{ik}^{(\mu)} (X_{\mu k} - X_{\mu,k-1})$$

The stepped curves for the shear flow in the individual longitudinal strips calculated in this manner for Q = 1,700 kg (3,749 lb.), are adjusted by the continuous curves with the same integral value and therefrom the values of shear flow are obtained for the various sections where measurements were made. They are shown in figure 14. Because the longitudinal stiffness of the skin is concentrated in the stiffeners, the shear flow in the transverse direction remains constant within a panel. By comparison with the shear flows which were obtained from the measurements, one sees that these constant shear flows, in general, show the same distribution. Since the determination of the shear flow from the measured values is subject to inaccuracies because of the scatter, so the deviations are much greater than in the case of the comparison of the measured and calculated longitudinal stresses.

From the preceding calculations, an estimate can be made of the effect of the buckling of the skin at the fixed end on the stress distribution. The loading terms at the fixed end increase with a decrease in the shear stiffness sG; the coefficients in the equation, however, do not increase in the same rate because in the contribu-

tion from the stiffeners and frames the smaller effective widths of skin cannot work out so rapidly. Consequently, the values of the redundants become larger - that is, the distortion of the elementary distribution must be more marked at the fixed end after the buckling of the skin, as is confirmed in figure 11 by the measurements.

Loading case b, distributed transverse load on the webs: At the transverse frames 1, 2, 3, 4, and 5, a transverse load q is applied, half to each spar. The bending moment at the k^{th} frame amounts to

$$M_k = a \frac{(k-1)\,k}{2} q$$

The shear flow in the k^{th} transverse strip, according to the elementary bending theory, for q = 1 kg amounts to

$$t_{4k}^{(o)} = -\frac{1}{2} \frac{F_5 z_5}{J} \left(\frac{M_k - M_{k-1}}{a} \right)$$

$$t_{3k}^{(o)} = -\frac{\frac{1}{2} F_5 z_5 + F_4 z_4}{J} \left(\frac{M_k - M_{k-1}}{a} \right)$$

etc.

These differ from the former values in loading case a) only by the factor $1/a\,(M_k - M_{k-1})$. For the redundants at each intermediate frame, loading terms arise from the shear in the sheet and frames, which can be combined with the former values on the basis of relations between the shear flows. If we designate the former values with the index E, then we obtain (for q = 1 kg) a contribution from the shear in the sheet.

$$\delta_{ko}^{(B)} = (\delta_{60})_E \left(\frac{M_k - M_{k-1}}{a} - \frac{M_{k+1} - M_k}{a} \right)$$

$$= -\frac{1}{a} (M_{k-1} - 2M_k + M_{k+1}) (\delta_{60})_E$$

and after introducing the above expressions for M_k:

$$\delta_{ko}^{(B)} = - (\delta_{6o})_E \quad \text{for} \quad k = 1, 2, 3, 4, 5$$

$$\delta_{6o}^{(B)} = + 5 (\delta_{6o})_E$$

For the contribution from the cross frames, one finds, correspondingly:

$$\delta_{ko}^{(S)} = \frac{1}{a} (M_{k-2} - 4M_{k-1} + 6M_k - 4M_{k+1} + M_{k+2}) (\delta_{1o})_E$$

This value differs for $k = 2, 3, 4$; in comparison, it is

$$\delta_{1o}^{(S)} = \delta_{5o}^{(S)} = - \delta_{6o}^{(S)} = - (\delta_{1o})_E$$

The loading terms so determined and the corresponding solutions of the equations of elasticity for $q = 1$ kg are contained in tables IV to VII and IX. For the load $q = 340$ kg (750 lb.), the final stiffener stresses calculated by superposition are plotted in figure 18 and are compared with the average values from the measured stresses. The distribution of shear flow, determined as in the loading case a) is shown in figure 15. Also in this loading case, the results of the statical indeterminate calculations are satisfied by the measurements. The variations at the built-in end rest partly on the variations in the measured stresses and partly on the neglected coupling of the redundants in the statically indeterminate calculations.

3. Stress Distribution in the Case of Pure Bending Moment Introduced by Couples

The departures from the elementary stress distribution in these loading cases (figs. 6c and 6d) arise through the introduction of concentrated forces in the stiffened sheet of the compression side. At the point of application of the load, the departure is recognized as the difference between the actual and the elementary distribution of forces. This equilibrium group can be received into groups of the form of the orthogonal redundants which have, as a result, independent of one another, a decreasing curve of the corresponding redundant in the interior of the shell. The decrease can be calculated for each redundant according to equations solved in section III,3 of E-K. Therein, if the transverse stiffness is assumed uniformly distributed (lim-

iting case of cross frames spaced infinitesimal distances apart), one obtains a continuous curve of characteristic force groups dependent on the longitudinal coordinate x (calculated, out from the loaded cross section).

Next, the curve of the redundants is calculated if the equilibrium groups Γ_1, Γ_2, Γ_3, Γ_4 from the components of the characteristic force groups $\underline{X}_{1k}$, $\underline{X}_{2k}$, $\underline{X}_{3k}$, $\underline{X}_{4k}$ (see table III) act at the free end (x = 0). For the characteristic force group $\underline{X}_1$

$$\kappa_L = \frac{\kappa_L}{a_2} = 0.2238; \quad \kappa_S \bar{\omega}_S = a^2 \kappa_S \omega_S = 4.84 \times 10^6$$

therefore, according to equations (28') and (29') of E-K:

$$\frac{\bar{\psi}}{\rho} = \sqrt{\frac{\kappa_B \omega_B}{\kappa_S \bar{\omega}_S} \pm \sqrt{\frac{4\bar{\kappa}_L}{\kappa_S \bar{\omega}_S}}} = \begin{cases} 0.0320; \\ 0.0128 \end{cases} \quad \bar{\varphi} = \sqrt{\frac{4\bar{\kappa}_L}{\kappa_B \omega_B}} = 0.01766$$

With this one obtains, according to equations (27') and (29') of E-K, the curve of the redundants for the application of the equilibrium group Γ_1 at the end cross section:

$$X_1(x) = e^{-0.0320\,x}(\cosh 0.0128\,x + 2.50 \sinh 0.0128\,x) \qquad (7)$$

in the case of frames elastic in the transverse direction.

$$X_1(x) = e^{-0.0320\,x}(\cosh 0.0128\,x + 1.45 \sinh 0.0128\,x) \qquad (7')$$

in the case of a rigid frame at 0 and elastic intermediate frames,

$$X_1(x) = e^{-0.01766\,x} \qquad (7'')$$

in the case of rigid frames. The curve of the characteristic force group of higher order can be computed under the assumption of rigid frames. (See E-K, example no. 1). Thus one obtains:

$$\left.\begin{aligned} X_2(x) &= e^{-0.0346x} \\ X_3(x) &= e^{-0.0486x} \\ X_4(x) &= e^{-0.0567x} \end{aligned}\right\} \quad \ldots\ldots\ldots\ldots (8)$$

The curves for this characteristic force group according to these formulas are plotted against the shell length in figure 19. The values become negligibly small at the built-in end of the shell ($x = 323.5$ cm (127.3 in.), so that the above equations valid for infinitely long shells can be used.

Loading case c, couples applied to the spars: Figure 20 shows the forces introduced in the chords of the spars for a load less than that producing buckling. The total bending moment introduced amounts to $M_B = 2{,}714$ mkg (235,500 in.-lb.). The forces $P_i^{(o)}$ of the elementary distribution are obtained from

$$P_i^{(o)} = \frac{M_B}{J} z_i F_i$$

with the values of z_i from table I,b and $J = 24{,}300$ cm^4 (584 in.^{4}). The equilibrium group, which represents the difference between the two distributions, is resolved into an equilibrium group Γ, whose longitudinal forces in the stiffeners of the compression side form within itself an equilibrium system, and small additional moments in the chords of the spars which are in equilibrium with the superimposed forces of the curved compression side. (See fig. 13 of E-K.)

Γ (with the partial forces $\bar{P}_i^{(o)}$) are resolved into the equilibrium groups Γ_1 to Γ_4 from the partial forces $P_i^{(\mu)}$ of the characteristic force groups $\underline{X}_\mu$:

$$\Gamma = c_1 \Gamma_1 + c_2 \Gamma_2 + c_3 \Gamma_3 + c_4 \Gamma_4 \qquad (9)$$

The development coefficient c_μ is obtained regarding the orthogonality relation

$$\sum_{i=1}^{9} P_i^{(\mu)} P_i^{(\nu)} = 0$$

for $\mu \neq \nu$ according to equation (26) of E-K

$$\left(\sum_{i=1}^{9} P_i^{(\mu)} \, P_i^{(\mu)} = \frac{9}{2} \right)$$

$$c_\mu = \frac{1}{4.5} \sum_{i=1}^{9} \bar{P}_i^{(o)} \, P_i^{(\mu)}$$

After inserting the numerical values from figure 20 and table III, it is found that

$$c_1 = + 1{,}528; \quad c_2 = - 1{,}103; \quad c_3 = + 800; \quad c_4 = - 207$$

Let it be assumed that Γ exerts the principal effects of the equilibrium group; the additional moments from the curvature of the shell fade away over the length of the shell approximately as the characteristic force group of the first order. The redundants resulting from Γ are obtained by multiplication of the values in figure 19 with the corresponding constant c_μ. For X_1, the values from (7) (elastic transverse frames) are to be used because at the free edge of the loaded side no transverse stiffness of the compression skin is present. If one superposes now the elementary distribution of the longitudinal forces resulting from these redundants, then the final distribution of forces is obtained, and from this the corresponding stress relations which are shown in figure 21.

The comparison with the test results gives a good agreement for stiffeners 3 to 7. In stiffeners 2 and 8 the measured stress in the first panel is not as high as obtained by computation. The stresses in the chords of the spars fade away correspondingly more slowly. These variations rest for the most part on the coupling of the redundants by the nonuniform cross sections of the stiffeners, because the characteristic force groups used are orthogonal only with equal stiffeners. If one sets up the orthogonal characteristic force groups belonging to the actual cross sections of the stiffeners of the model according to the general procedure outlined in section III,2 of E-K, and carries through the computations, then one obtains the stress curves shown as dot-dash lines in figure 21, which show good agreement with the measured values.

For the calculation of the shear flow at the cross sections where measurements were made, one first determines the values

$$\frac{dP_i}{dx} = P_i^{(1)} X_1' + P_i^{(2)} X_2' + P_i^{(3)} X_3' + P_i^{(4)} X_4'$$

at these places whereat one obtains the derivative X_μ' by differentiation of (7) and (8) and multiplication with the corresponding constant c_μ. Then

$$t_4(x) = \frac{1}{2} \frac{dP_4}{dx}$$

$$t_3(x) = \frac{1}{2} \frac{dP_4}{dx} + \frac{dP_3}{dx}$$

etc.

The results of the numerical calculations are plotted in figure 16. One obtains essentially the same distribution of shear as given by the measured values, to be sure, with greater variations as in the loading cases with transverse bending forces.

Loading case d, couples applied at the middle of the wing: The couple had the same moment M = 2,714 mkg (235,500 in.-lb.) as in the previous loading case; therefore, it gives the same elementary distribution of forces. The compressive force of 7,050 kg (15,545 lb.) is applied through the attachment in figure 5 to stiffeners 4, 5, and 6, whereat the distribution to the individual stiffeners depends on the flexibility of the attachment. In order to avoid the determination of this distribution from a statically indeterminant calculation, it was assumed as corresponding to the results of the measured stresses in cross section VII α'. (See fig. 2.) One therefore obtains the forces given in figure 22 at stiffeners 4, 5, and 6.

The method of calculation is exactly the same as for the preceding loading case. As development coefficients of the equilibrium group Γ, one obtains the values:

$$c_1 = - 1,296; \quad c_2 = - 700; \quad c_3 = - 157; \quad c_4 = + 301$$

For the fading out of X_1, equation (7') (rigid end frame) is chosen because an appreciable stiffening in the transverse direction is produced by the attachment at the center. The additional moment in the spars resulting from the curvature of the sheet should decrease as the force group X_1 in the longitudinal direction.

Figure 23 contains the results of the numerical calculation for the stresses in the individual longitudinal stiffeners. Also here there is good agreement with the measured values. The corresponding distribution of shear flow is shown in figure 17; the stepped curve of the calculated shear flow over the cross section furnishes thereby useful average values for the shear loading of the individual stiffeners.

V. SUMMARY

By means of strain measurements in a hollow wing model, the longitudinal stresses in the compression side resulting from loadings with transverse loads and pure bending were determined and plotted in perspective in the form of stress peaks on the outline. It was found that the calculations of such a framework according the elementary bending theory which neglects the effects of shear strains, may result in only a first approximation.

Through the shear deformations of the effective width of skin covering, distortions of the cross section arise with bending produced by transverse loads whose restraint at the built-in end had as a result an unloading of the interior longitudinal stiffeners and a correspondingly higher loading of the chords of the spars. In the practically important cases of distributed load over the length of the member, these superposed stresses can amount to more than 30 percent of the elementary stress distribution. Small differences occur also at the points of application of the transverse loads.

In the case of loading through pure bending by means of couples, concentrated forces were introduced into the shell construction as they occur practically at the points of attachment of the shell wings. Also in this case, the elementary stress distribution was distorted by secondary stresses. In the model studied, these distortions of stress extended in the longitudinal direction from the point of application of the load for a distance of about 1.5 times the width of the shell.

Exceeding the buckling limit of the skin covering changed the stress distribution in the longitudinal stiffeners only slightly. In the case of bending under transverse loads, the distortion of the stress at the built-in end increased somewhat as a result of the decreased shear

stiffness of the skin. In general, the stresses in the longitudinal stiffeners increased because of the decreased effectiveness of the skin with respect to longitudinal forces.

From the longitudinal stresses measured before buckling, the distribution of the shear flow was calculated in order to obtain a picture of the shear loading in the skin introduced by that kind of stress distortion.

The loading cases studied were treated theoretically; also, under the assumption that the skin between longitudinal and transverse stiffeners resisted only shear. The carrying out of the statically indeterminant calculations was done according to the procedure established by Ebner and Köller in an earlier work (Luftfahrtforschung, vol. 15, 1938, pp. 527-542). The values of stress determined mathematically have good agreement with the measured values so that the "shear field theory" represents a usable idealization for the calculation of that kind of stiffened shell construction.

Translation by Marshall Holt,
Aluminum Research Laboratories,
Aluminum Company of America.

REFERENCES

1. Ebner, H.: Zur Festigkeit von Schalen- und Rohfholmflügeln. Luftfahrtforschung, vol. 14, 1937, pp. 179-190.

2. Doetsch, H.: Profilwiderstandsmessungen im grossen Windkanal der D.V.L. Luftfahrtforschung, vol. 14, 1937, pp. 173-178.

3. Schapitz, E., and Krümling, G.: Load Tests on a Stiffened Circular Cylindrical Shell. T.M. No. 864, N.A.C.A., 1938.

4. Ebner, H., and Köller, H.: Über den Kraftverlauf in längs- und querversteiften Scheiben. Luftfahrtforschung, vol. 15, 1938, pp. 527-542.

5. Ebner, H., and Köller, H.: Calculation of Load Distribution in Stiffened Cylindrical Shells. T.M. No. 866, N.A.C.A., 1938.

6. Lovett, B. B. C., and Rodee, W. F.: Transfer of Stress from Main Beams to Intermediate Stiffeners in Metal Sheet Covered Box Beams. Jour. of the Aero. Sciences, vol. 3, October 1936, p. 426.

7. Chwalla, E.: Theory of the Stability of Web Plates of Thin-Walled Beams. Stahlbau, vol. 9, 1936, pp. 161-166.

8. Ebner, H.: The Strength of Shell Bodies - Theory and Practice. T.M. No. 838, N.A.C.A., 1937.

TABLE IV

Equations of Elasticity for the Redundants $\underline{X}_{1k}$

k	$X_{1.1}$	$X_{1.2}$	$X_{1.3}$	$X_{1.4}$	$X_{1.5}$	$X_{1.6}$	Loading case a) $C\delta_{k_o}^{(1)}$	Loading case b) $C\delta_{k_o}^{(1)}$
1	10.14	-4.44	0.48	-	-	-	-0.155	0.963
2	-4.44	10.14	-4.44	0.48	-	-	0	.808
3	.48	-4.44	10.14	-4.44	0.48	-	0	.808
4	-	.48	-4.44	10.14	-4.44	0.48	0	.808
5	-	-	.48	-4.44	9.66	-3.48	0	.963
6	-	-	-	.48	-3.48	4.11	-.808	-4.195

TABLE V

Equations of Elasticity for the Redundants $\underline{X}_{2k}$

k	$X_{2.1}$	$X_{2.2}$	$X_{2.3}$	$X_{2.4}$	$X_{2.5}$	$X_{2.6}$	Loading case a) $C\delta_{k_o}^{(2)}$	Loading case b) $C\delta_{k_o}^{(2)}$
1	3.409	-0.518	0.027	-	-	-	0.0272	-0.1924
2	-.518	3.409	-.518	0.027	-	-	0	-.1652
3	.027	-.518	3.409	-.518	0.027	-	0	-.1652
4	-	.027	.518	3.409	-.518	0.027	0	-.1652
5	-	-	.027	-.518	3.382	-.464	0	-.1924
6	-	-	-	.027	-.464	1.650	.1652	.8532

TABLE VI

Equations of Elasticity for the Redundants X_{3k}

k	$X_{3.1}$	$X_{3.2}$	$X_{3.3}$	$X_{3.4}$	$X_{3.5}$	$X_{3.6}$	Loading case a) $C\delta^{(3)}_{k_o}$	Loading case b) $C\delta^{(3)}_{k_o}$
1	2.683	-0.025	0.004	-	-	-	-0.0093	0.0753
2	-.025	2.683	-.025	0.004	-	-	0	.0660
3	.004	-.025	2.683	-.025	0.004	-	0	.0660
4	-	.004	-.025	2.683	-.025	0.004	0	.0660
5	-	-	.004	-.025	2.679	-.017	0	.0753
6	-	-	-	.004	-.017	1.333	-.0660	-.3393

TABLE VII

Equations of Elasticity for the Redundants X_{4k}

k	$X_{4.1}$	$X_{4.2}$	$X_{4.3}$	$X_{4.4}$	$X_{4.5}$	$X_{4.6}$	Loading case a) $C\delta^{(4)}_{k_o}$	Loading case b) $C\delta^{(4)}_{k_o}$
1	2.555	0.114	0.001	-	-	-	0.0025	-0.0159
2	.114	2.555	.114	0.001	-	-	0	-.0134
3	.001	.114	2.555	.114	0.001	-	0	-.0134
4	-	.001	.114	2.554	.114	0.001	0	-.0134
5	-	-	.001	.114	2.554	.116	0	-.0159
6	-	-	-	.001	.116	1.275	-.0134	.0695

TABLE VIII

Shear Flow and Force in Transverse Frames Resulting from Bending Under Unit Transverse Load $\bar{Q}$ = 1 kg (2.2 lb.) at Free End (load case a)) and the Static Redundants

i	Shear flow					Forces in transverse frames				
	$Jt_{ik}^{(0)}$	$at_{ik}^{(1)}$	$at_{ik}^{(2)}$	$at_{ik}^{(3)}$	$at_{ik}^{(4)}$	$\frac{J}{b} Q_{o,i+1}^{(0)}$	$R_{k,i+1}^{(1)}$	$R_{k,i+1}^{(2)}$	$R_{k,i+1}^{(3)}$	$R_{k,i+1}^{(4)}$
1	-243.1	0.940	-0.766	0.500	-0.174	243.1	0.940	-0.766	0.500	-0.174
2	-181.2	1.440	-.266	-.500	.326	424.3	2.380	-1.032	0	.152
3	-114.7	1.266	.674	0	-.440	539.0	3.646	-.358	0	-.288
4	-45.5	.500	.500	.500	.500	584.5	4.146	.142	.500	.212

TABLE IX

Static Redundants Resulting from Bending by Transverse Forces

k	Loading case a) Transverse load at the free end of the web ($\bar{Q}$ = 1 kg (2.2 lb.))				Loading case b) Distributed transverse load (q = 1 kg (2.2 lb.))			
	X_{1k}	X_{2k}	X_{3k}	X_{4k}	X_{1k}	X_{2k}	X_{3k}	X_{4k}
1	0.0217	-0.0082	0.0035	-0.0010	-0.199	0.066	-0.028	0.006
2	.0172	-.0013	.0000	-.0000	-.264	.068	-.025	.005
3	.0233	-.0002	.0000	.0000	-.241	.068	-.025	.005
4	.0526	-.0014	.0000	-.0000	-.083	.062	-.025	.005
5	.1315	-.0145	.0003	.0005	.343	-.005	-.027	.006
6	.3012	-.1041	.0495	-.0105	1.301	-.519	.254	-.054

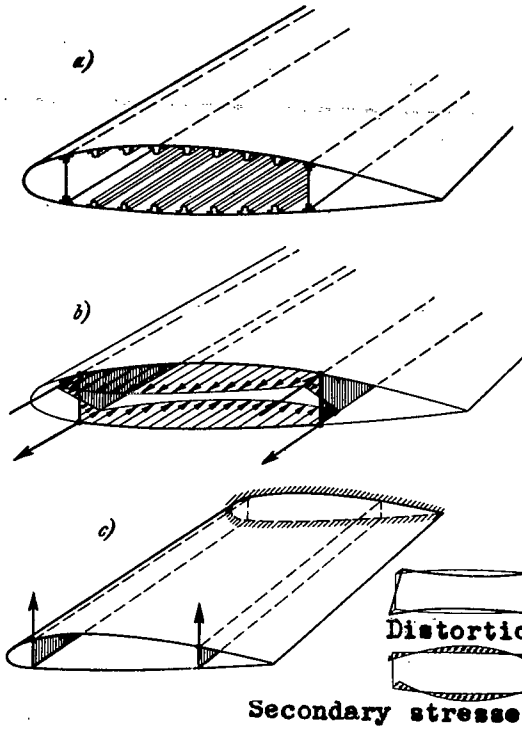

(a) Sketch of monocoque wing.
(b) Distribution of stresses in the case of loading by couples at the spar chords.
(c) Loading by transverse forces at the spars.

Figure 1. Statement of the problem.

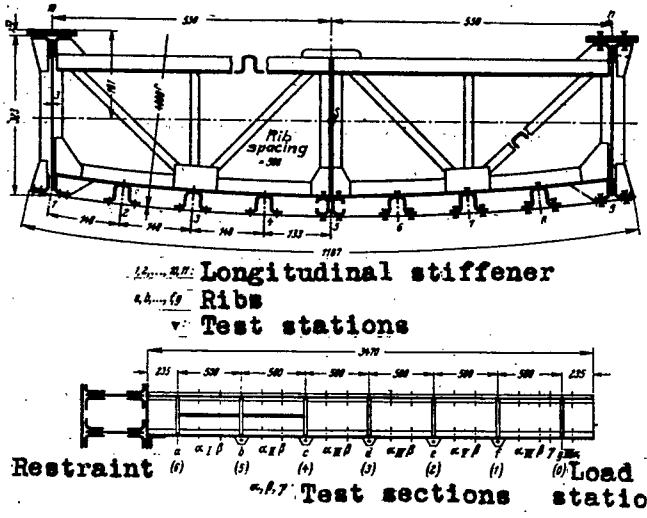

Figure 2.- Transverse section and longitudinal view of the wing model studied. Position of measurement stations.

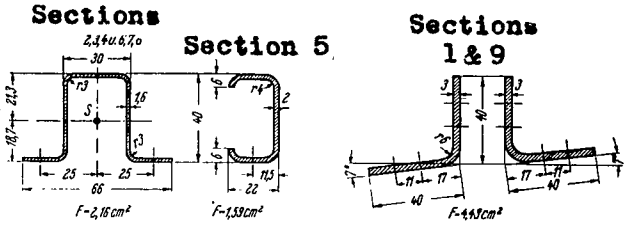

Figure 3.- Dimensions of the longitudinal stiffeners on the compression skin.

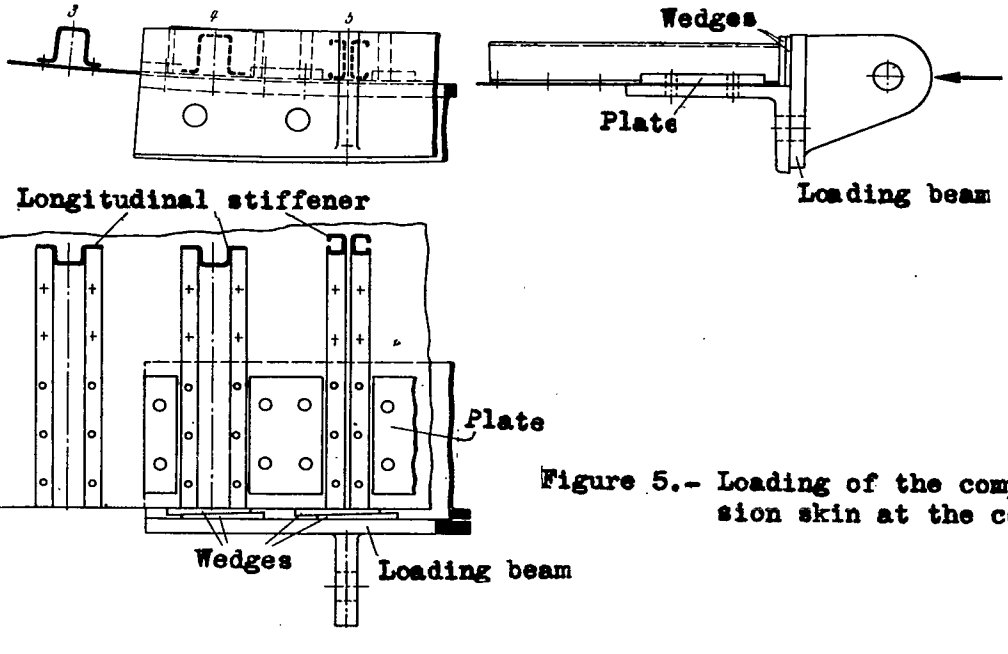

Figure 5.- Loading of the compression skin at the center.

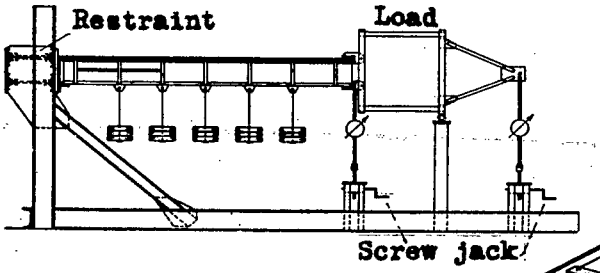

Figure 4.- Test set up.

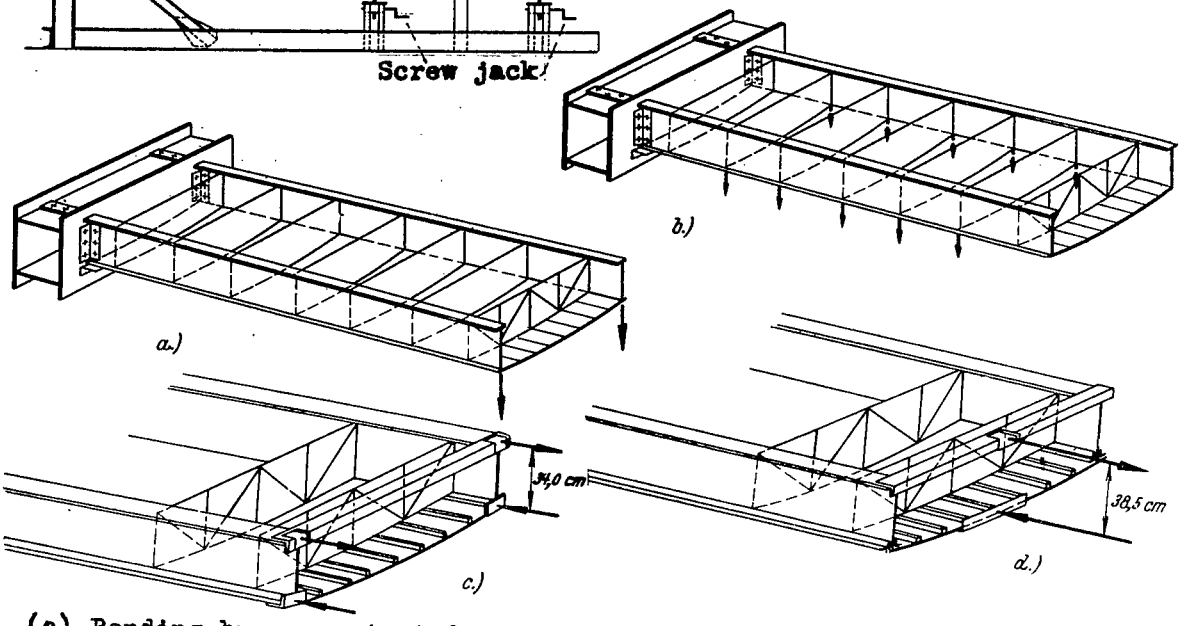

(a) Bending by concentrated transverse forces at the ends of the webs
(b) Bending by uniformly distributed transverse forces on the webs
(c) Pure bending by couples at the spar chords
(d) Pure bending by a couple at the center of the wing

Figure 6.- Loading cases studied.

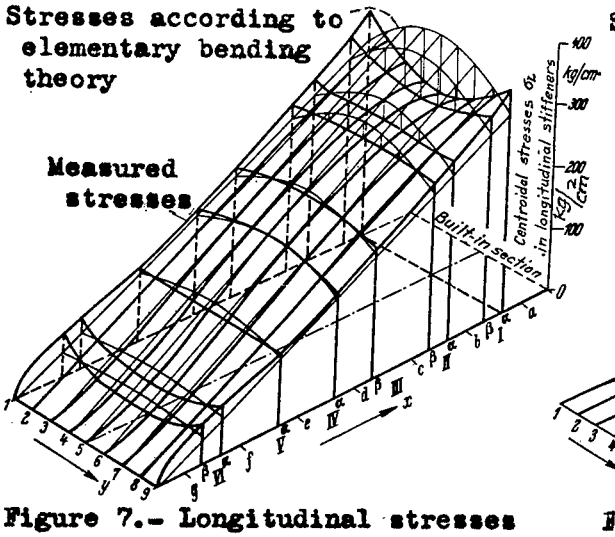

Figure 7.- Longitudinal stresses in the case of bending with a concentrated transverse force at the ends of the webs (Figure 6a, total transverse load force Q= 1700 kg [3760 lb.]).

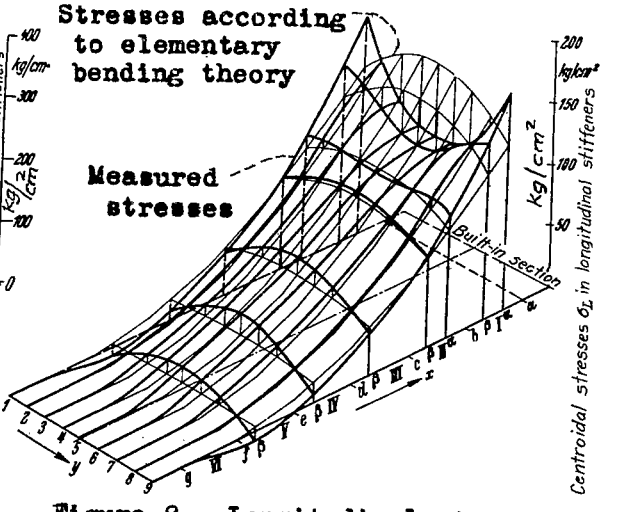

Figure 8.- Longitudinal stresses in the case of bending by uniformly distributed loads on the webs (Figure 6b, total transverse load $\bar{Q}$ = 1700 kg [3760 lb.]).

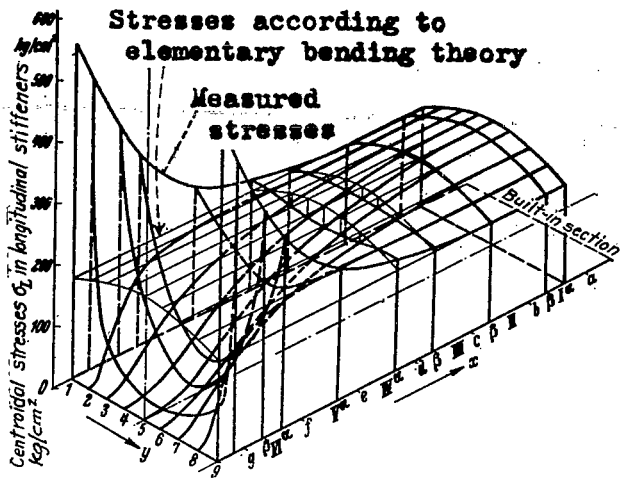

Figure 9.- Longitudinal stresses in the case of pure bending by couples at the spar chords (Figure 6c, total moment $M_B = 2714$ mkg [235,500 in.-lb.]).

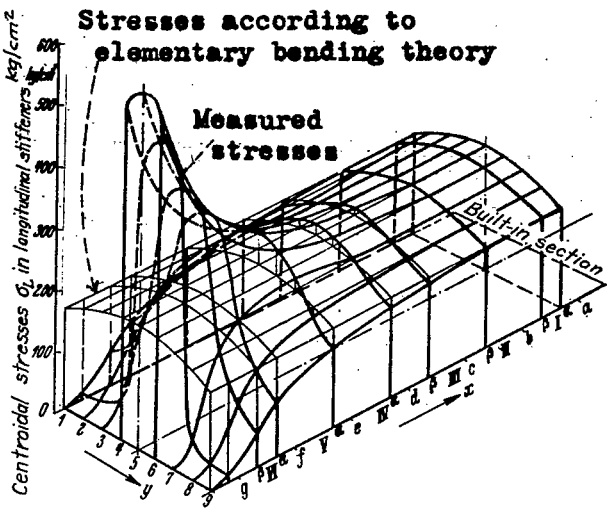

Figure 10.- Longitudinal stresses in the case of pure bending by a couple at the middle of the wing (Figure 6d, moment $M_B = 2714$ mkg [235,500 in.-lb.]).

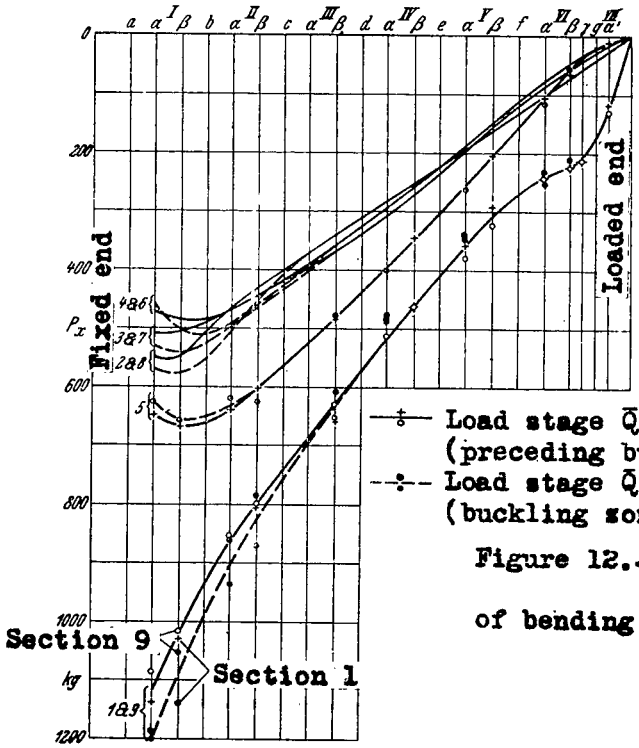

Figure 11.- Effect of buckling of the skin on the stress distribution in the case of bending by transverse loads at the free ends of the webs.

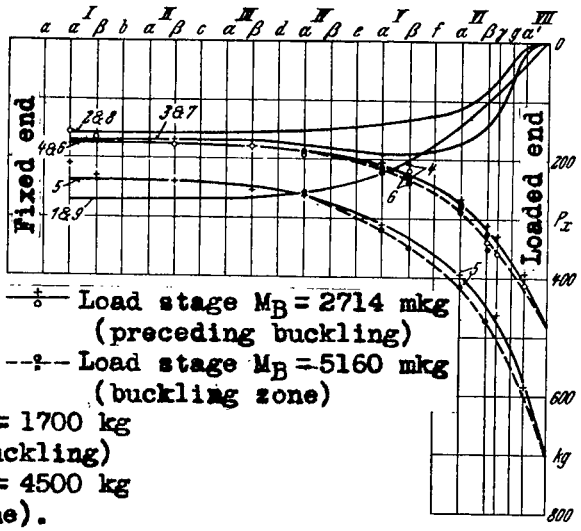

Figure 12.- Effect of buckling of the skin on the stress distribution in the case of bending by a couple at the middle of the wing.

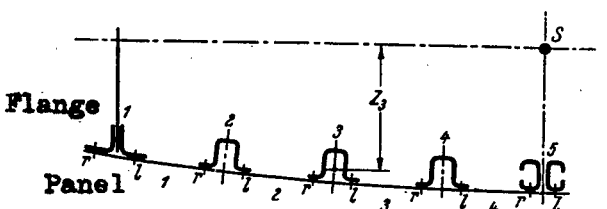

Figure 13.- Designation of the panels in the skin.

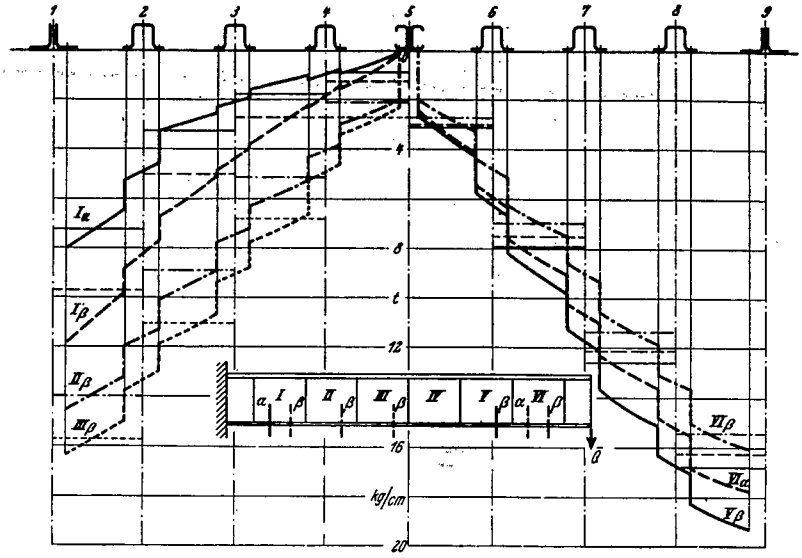

Figure 14.- Shear flow in the case of bending by concentrated loads at free ends of the webs (total transverse load, $\bar{Q}$ = 1700 kg [3760 lb.] heavy curve: shear flow determined from the strain measurements. Light horizontal lines: calculated values.)

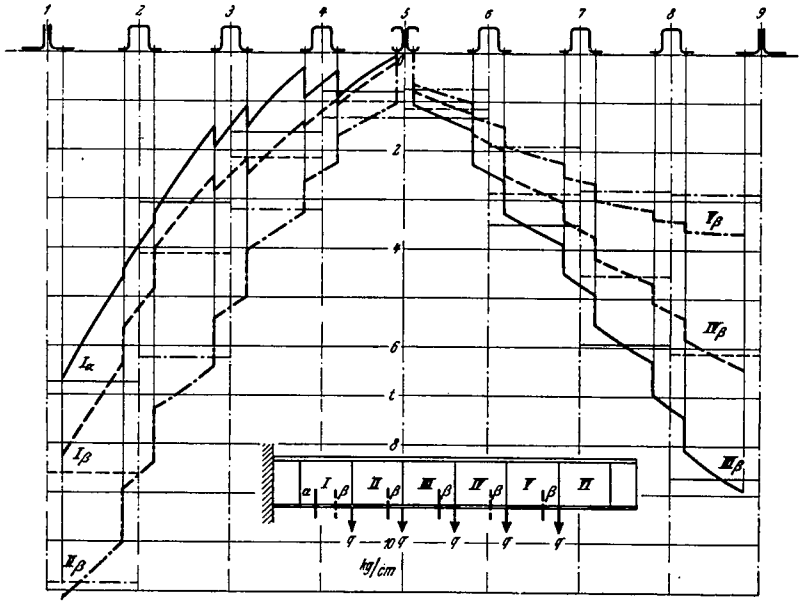

Figure 15.- Shear flow in the case of bending by uniformly distributed transverse loads on the webs. Total transverse load $\bar{Q}$ = 1700 kg [3760 lb.] heavy curve: shear flow determined from the strain measurements. Light horizontal lines: calculated values.

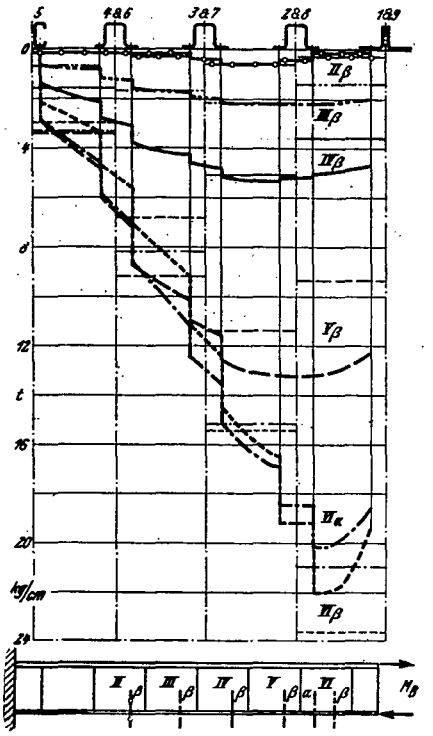

Figure 16.- Shear flow in the case of pure bending by couples at spar chords. Total bending moment M_B = 2714 mkg [235,500 in.-lb.] heavy curve: shear flow determined from strain measurements. Light horizontal lines: calculated values

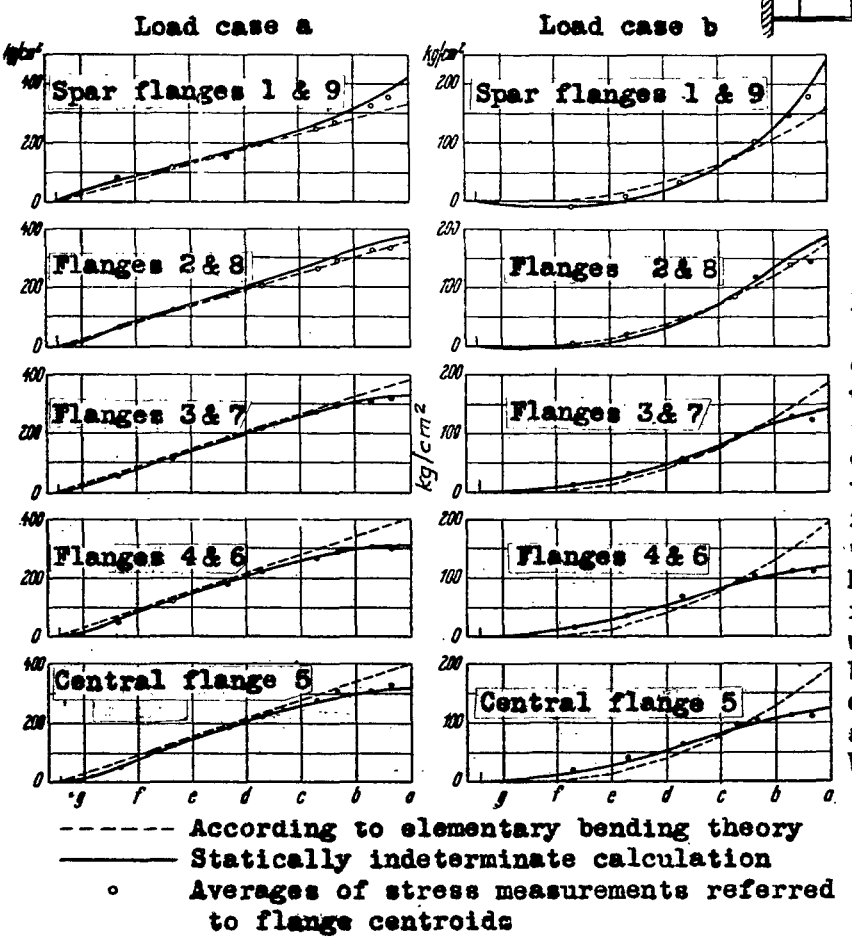

Figure 18.- Comparison of calculated and measured longitudinal stresses in the case of bending by transverse forces. Loading case a: Transverse load $\bar{Q}$ = 1700 kg [3760 lb.] at the free ends of the webs. Loading case b: Transverse load q = 340 kg [750 lb.] on transverse frames b,c,d,e,and f.

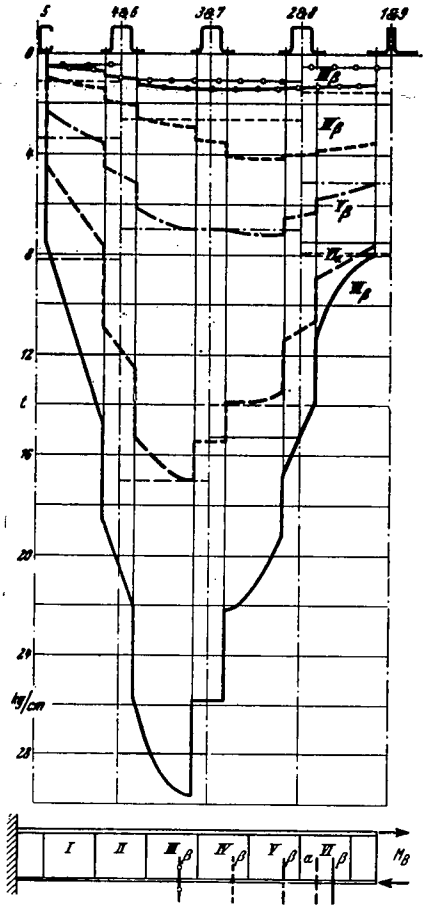

Figure 17.- Shear flow in the case of bending by a couple at the middle of the wing (moment M_B = 2714 mkg [235,500 in.-lb.] heavy curve: shear flow determined from the strain measurements. Light horizontal lines: calculated values).

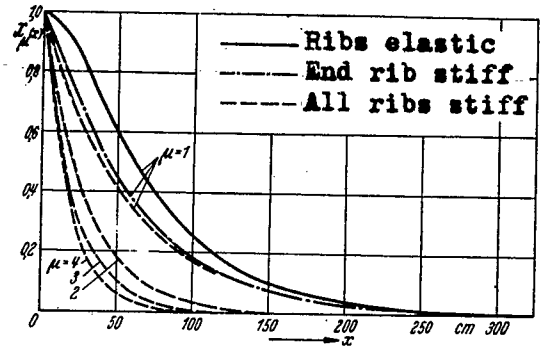

Figure 19.- Decrease of the equilibrium force groups Γ_μ introduced by the distributed forces of the redundants $\bar{X}_\mu$.

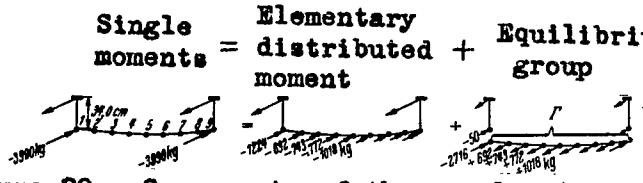

Figure 20.- Components of the couples introduced into the spar chords (total bending moment M_B = 2714 mkg [235,500 in.-lb.]).

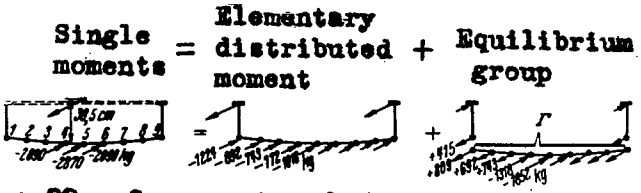

Figure 22.- Components of the couple introduced at the middle of the wing (moment M_B = 2714 mkg [235,500 in.-lb.]).

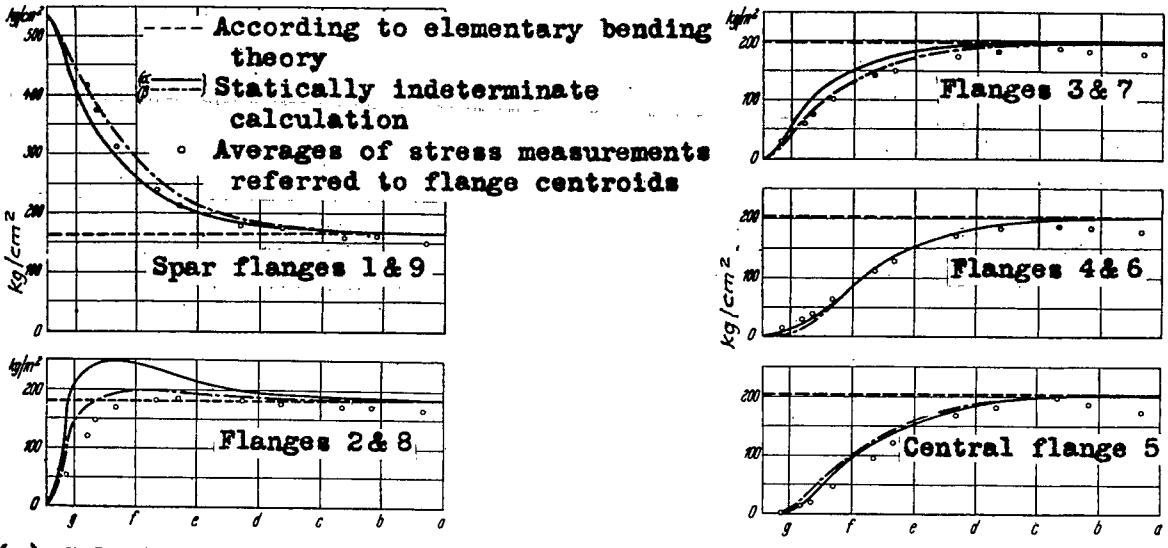

(α) Calculated by means of orthogonal characteristic force groups for sheets with equal stiffeners.

(β) Calculated by means of exact orthogonal characteristic force groups of the model.

Figure 21.- Comparison of the calculated and measured longitudinal stresses in the case of couples introduced in the spar chords.
Loading case c: total moment M_B = 2714 mkg [235,500 in.-lb.]

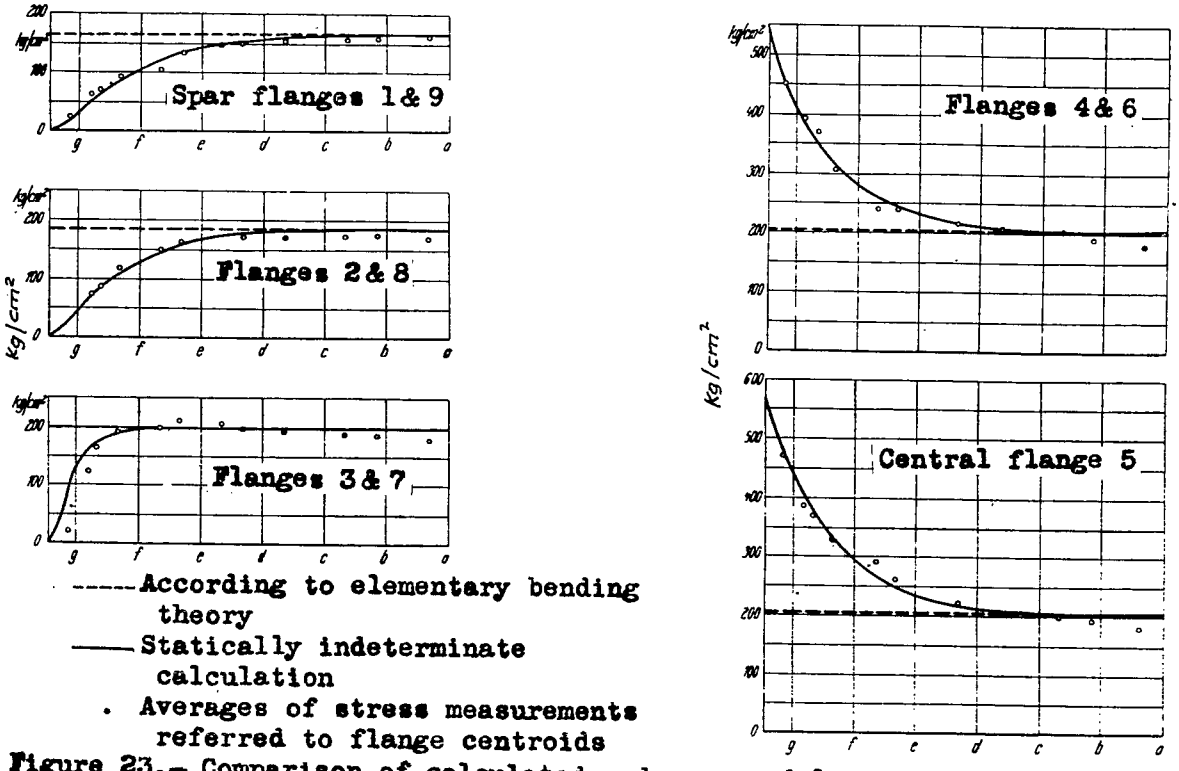

-----According to elementary bending theory

——Statically indeterminate calculation

. Averages of stress measurements referred to flange centroids

Figure 23.- Comparison of calculated and measured longitudinal stresses in the case of a couple introduced at the middle of the wing.
Loading case d: Moment M_B = 2714 mkg [235,500 in.-lb.]